Probing Catalysis by Escherichia coli dTDP-Glucose-4,6-dehydratase: Identification and Preliminary Characterization of Functional Amino Acid Residues at the Active Site †

ARTICLE *in* BIOCHEMISTRY · JULY 2001

Impact Factor: 3.02 · DOI: 10.1021/bi010441a · Source: PubMed

3 AUTHORS, INCLUDING:

Adrian Hegeman
University of Minnesota Twin Cities
77 PUBLICATIONS **2,262** CITATIONS
SEE PROFILE

Perry Allen Frey
University of Wisconsin–Madison
302 PUBLICATIONS **10,242** CITATIONS
SEE PROFILE

Probing Catalysis by *Escherichia coli* dTDP-Glucose-4,6-dehydratase: Identification and Preliminary Characterization of Functional Amino Acid Residues at the Active Site†

Adrian D. Hegeman,‡ Jeffrey W. Gross,‡ and Perry A. Frey*

Department of Biochemistry, University of Wisconsin−Madison, Madison, Wisconsin 53705

Received March 5, 2001; Revised Manuscript Received April 11, 2001

ABSTRACT: A model of the *Escherichia coli* dTDP-glucose-4,6-dehydratase (4,6-dehydratase) active site has been generated by combining amino acid sequence alignment information with the 3-dimensional structure of UDP-galactose-4-epimerase. The active site configuration is consistent with the partially refined 3-dimensional structure of 4,6-dehydratase, which lacks substrate−nucleotide but contains NAD^+ (PDB file 1BXK). From the model, two groups of active site residues were identified. The first group consists of $Asp135^{DEH}$, $Glu136^{DEH}$, $Glu198^{DEH}$, $Lys199^{DEH}$, and $Tyr301^{DEH}$. These residues are near the substrate−pyranose binding pocket in the model, they are completely conserved in 4,6-dehydratase, and they differ from the corresponding equally well-conserved residues in 4-epimerase. The second group of residues is $Cys187^{DEH}$, $Asn190^{DEH}$, and $His232^{DEH}$, which form a motif on the *re* face of the cofactor nicotinamide binding pocket that resembles the catalytic triad of cysteine-proteases. The importance of both groups of residues was tested by mutagenesis and steady-state kinetic analysis. In all but one case, a decrease in catalytic efficiency of approximately 2 orders of magnitude below wild-type activity was observed. Mutagenesis of each of these residues, with the exception of $Cys187^{DEH}$, which showed near-wild-type activity, clearly has important negative consequences for catalysis. The allocation of specific functions to these residues and the absolute magnitude of these effects are obscured by the complex chemistry in this multistep mechanism. Tools will be needed to characterize each chemical step individually in order to assign loss of catalytic efficiency to specific residue functions. To this end, the effects of each of these variants on the initial dehydrogenation step were evaluated using a the substrate analogue dTDP-xylose. Additional steady-state techniques were employed in an attempt to further limit the assignment of rate limitation. The results are discussed within the context of the 4,6-dehydratase active site model and chemical mechanism.

dTDP-Glucose-4,6-dehydratase[1,2] catalyzes the conversion of dTDP-glucose into dTDP-4-keto-6-deoxyglucose and was first identified in the biosynthesis of L-rhamnose (*1*). This and other 4,6-dehydratases catalyze the first committed step in all 6-deoxysugar biosynthetic pathways described to date (*2*). Numerous 6-deoxysugars are used in bacterial lipopolysaccharide production as well as in the biosynthesis of a diverse array of secondary metabolites (*3*−*5*).

The chemical mechanism for the 4,6-dehydratase is postulated to proceed through several steps (Scheme 1; reviewed in *6*) beginning with oxidation at glucosyl C4 by NAD^+, generating dTDP-4-ketoglucose and NADH. Water is then eliminated between glucosyl C5 and C6, presumably assisted by general acid−base catalysis, to form dTDP-4-ketoglucose-5,6-ene. Finally, the $\alpha-\beta$ unsaturated ketone is reduced by NADH at glucose C6, producing the product dTDP-4-keto-6-deoxyglucose and regenerating NAD^+. Our recent characterization of a single-turnover reaction catalyzed by 4,6-dehydratase by rapid mix-quench MALDI-TOF analysis fully supports this mechanism by showing the transient appearance and kinetic competence of the dTDP-4-ketoglucose-5,6-ene (*7*).

The 4,6-dehydratase is physically and mechanistically similar to UDP-galactose-4-epimerase[3] (*8*, *9*). Both enzymes

† This work was supported by Grants GM30480 (P.A.F.) and GM20552 (J.W.G.) from the National Institute of General Medical Sciences.

* Correspondence should be addressed to this author at the University of Wisconsin−Madison, 1710 University Ave., Madison, WI 53705. Tel: (608) 262-0055. Fax: (608) 265-2904. E-mail: frey@biochem.wisc.edu.

‡ Both authors have contributed equally to this work.

[1] Abbreviations: AaaXXX^{DEH}, amino acid Aaa sequence number *XXX* in 4,6-dehydratase; AaaXXX^{EPIM}, amino acid Aaa sequence number *XXX* in 4-epimerase; A*XXX*B^{DEH}, amino acid A sequence number *XXX* variant B in 4,6-dehydratase; CD, circular dichroism; 4,6-dehydratase, dTDP-glucose-4,6-dehydratase; dTDP-glucose, thymidine-5′-diphospho-α-D-glucose; dTDP-glucose-d_7, dTDP-[1,2,3,4,5,6,6-$^2H_7$]glucose; DTT, dithiothreitol; dTTP, thymidine-5′-triphosphate; EDTA, ethylenediaminetetraacetic acid; 4-epimerase, UDP-galactose-4-epimerase; HEPES, 4-(2-hydroxyethyl)piperazine-1-ethanesulfonic acid; MALDI-TOF MS, matrix-assisted laser desorption/ionization time-of-flight mass spectrometry; MOPS, 3-(*N*-morpholino)propanesulfonic acid; NAD^+, nicotinamide adenine dinucleotide (oxidized); NADD, [4-$^2H_1$]nicotinamide adenine dinucleotide (reduced); NADH, nicotinamide adenine dinucleotide (reduced); OD_{600}, optical density at 600 nm; ORF, open reading frame; P_i, inorganic phosphate; PDB, Protein Data Bank; PGM, phosphoglucomutase; PMSF, phenylmethanesulfonyl fluoride; TLC, thin-layer chromatography; TRIS, tris(hydroxymethyl)aminomethane; UDP, uridine-5′-diphosphate; wt, wild type.

[2] dTDP α-D-glucose 4,6-hydro-lyase, EC 4.2.1.46.

[3] UDP α-D-galactose 4-epimerase, EC 5.1.3.2.

10.1021/bi010441a CCC: $20.00
Published on Web 05/11/2001

Scheme 1

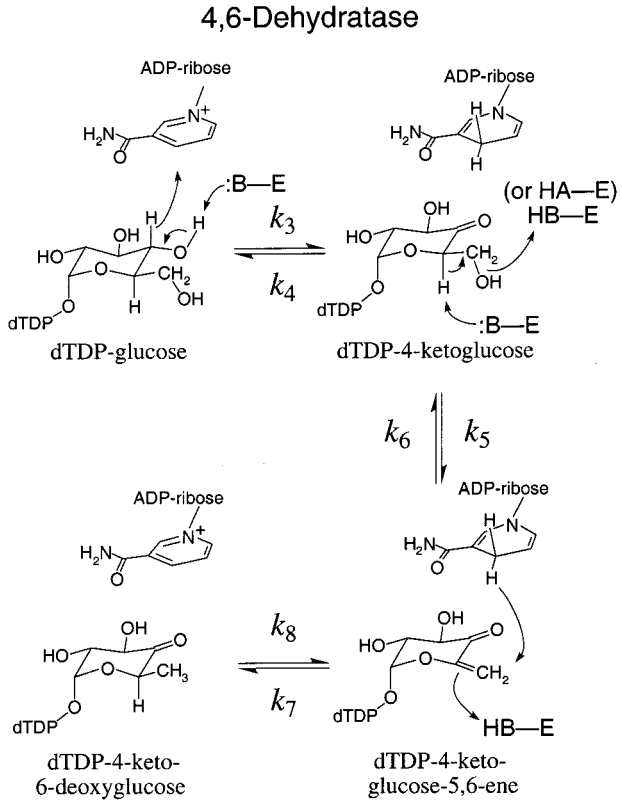

Scheme 2

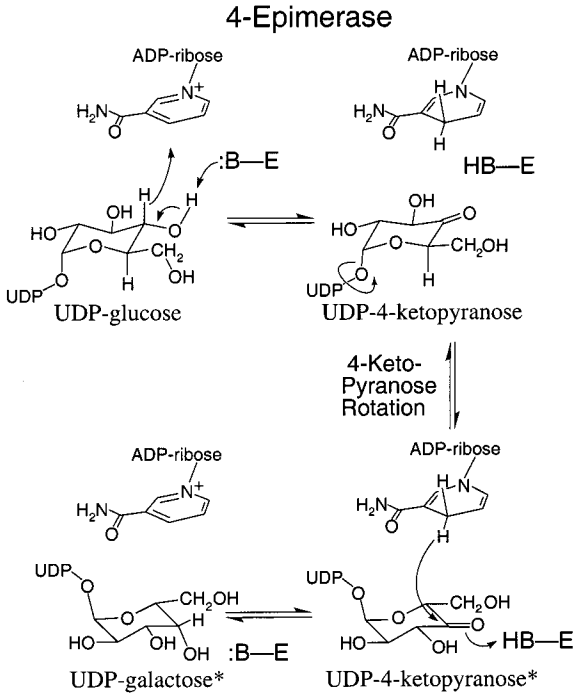

are members of the extended short chain dehydrogenase/reductase superfamily (*10*) that use nicotinamide dinucleotides to catalyze oxidoreductase chemistry. There is 25% amino acid sequence identity between 4-epimerase and 4,6-dehydratase, and they have similar three-dimensional structural folds (*11*; and PDB no. 1BXK). Both enzymes are homodimers, and each contains one irreversibly bound NAD^+ cofactor in each subunit (*7*, *12*). For both enzymes, catalysis begins with the same mechanistic step (compare Schemes 1 and 2), where tightly bound NAD^+ oxidizes carbon-4 in the hexopyranose moiety of the nucleotide−sugar substrate. The two mechanisms diverge following that step, as the 4-epimerase allows rotation of the 4-ketopyranose such that reduction of the keto-functionality by NADH may occur at either face to effect epimerization.

A great deal is known about the structure and function of the *E. coli* 4-epimerase, but little information of this kind has been reported for the 4,6-dehydratase. The reaction catalyzed by 4,6-dehydratase is a fairly complex three-step process (Scheme 1) that may be facilitated in many different ways at various stages by enzymatic means. While elegant experiments support the chemical and kinetic mechanism for 4,6-dehydratase (reviewed in *6*, *7*), the precise mechanism by which this enzyme directs catalysis is unknown.

Structural similarities between 4-epimerase and 4,6-dehydratase have here been used to generate a homology model of the 4,6-dehydratase active site. Two groups of active site residues in this model have been postulated to engage in the oxidoreduction and dehydration phases. The first group of residues, $Asp135^{DEH}$, $Glu136^{DEH}$, $Glu198^{DEH}$, $Lys199^{DEH}$, and $Tyr301^{DEH}$, is potentially involved in general acid/base catalysis of water elimination and the reduction of the dTDP-4-ketoglucose-5,6-ene intermediate. The second group, $Cys187^{DEH}$, $His232^{DEH}$, and $Asn190^{DEH}$, constitutes an interesting motif on the *re* face of the nicotinamide moiety of the NAD^+ (hydride transfer is to and from the *si* face) and might be important for modulating the reactivity of the cofactor. The kinetic and spectral consequences of altering these residues are reported in this paper and discussed in the context of the reaction mechanism.

EXPERIMENTAL PROCEDURES

Materials

Restriction endonucleases (except *Sap*I) and other DNA modifying enzymes were purchased from Promega; pCYB1 and *Sap*I were purchased from New England Biolabs. All deoxyoligonucleotides were obtained commercially (Cruachem, Dulles, VA) and further purified by urea denaturing acrylamide gel electrophoresis. Glycogen phosphorylase, hexokinase, phosphoglucomutase, and inorganic pyrophosphatase were purchased from Boehringer Manheim. UDP-glucose-pyrophosphorylase and glycogen were from Sigma. Carrier-free [^{32}P]orthophosphate (10 mCi/mL) and [γ-^{32}P]-ATP (6000 Ci/mmol) were purchased from Amersham. Sodium [^{3}H]borohydride (450 mCi/mmol) was purchased from American Radiolabeled Chemicals Inc. dTTP, dTMP-morpholidate, α-D-glucose-1-phosphate, and α-D-xylose-1-phosphate were purchased from Aldrich. Wt 4,6-dehydratase that was not purified using the affinity approach detailed below was obtained using a procedure outlined previously (*7*).

Methods

DNA sequencing was performed by the University of Wisconsin Biotechnology Center Nucleic Acid and Protein Facility. Nucleotide sugars: dTDP-α-D-xylose; dTDP-α-D-glucose; and dTDP-α-D-galactose, were synthesized from dTMP-morpholidate and α-D-xylose-1-phosphate, α-D-

glucose-1-phosphate, and α-D-galactose-1-phosphate respectively, and purified as previously described (*13*). Standard UV/Visible measurements were made using a Shimadzu UV-1601PC dual beam spectrophotometer or a Hewlett-Packard 8452A diode array spectrophotometer. NADH bound to 4,6-dehydratase was quantified using the extinction coefficient for the 4,6-dehydratase−NADH complex at 355 nm (ϵ_{355} = 6000 M^{-1} cm^{-1}; *7*). Pre-steady-state spectrophotometric traces were collected using an OLIS Inc. RSM-1000 stopped-flow spectrophotometer. Ion-paired reverse-phase HPLC was performed using a Waters Nova Pak C_{18} column with a 2 mL/min constant-flow rate, 20 min linear gradient from 100% solution A (2.5 mM tetrabutylammonium sulfate in 25 mM potassium phosphate, pH 6.0) to 80% solution B (80% acetonitrile). The column was pre-equilibrated with 200 mL of solution A prior to use. Analyte was detected upon elution using an in-line UV/Visible absorbance detector set to 267 nm. After each analysis, the column was washed with a 100% spike of solution B and re-equilibrated for 10 min with solution A. A Beckman LS 6500 multipurpose scintillation counter was used to quantify radioactivity.

Chitin Binding Protein/Intein/4,6-Dehydratase Fusion Expression Construct. The 4,6-dehydratase expression construct pTZ18UgalSDo355 (*7*) was modified by site-directed mutagenesis, using the Stratagene QuickChange kit as per instructions (primers are listed in the Supporting Information) to introduce a *Sap*I restriction site at the 3′ end of the 4,6-dehydratase ORF. Digestion of pCYB1 with *Sap*I and *Pst*I liberated a 1.55 kb DNA fragment that was cloned into the *Sap*I and *Pst*I sites of the modified 4,6-dehydratase expression construct. The ORF and flanking sequences of the resulting expression vector, pTZ18UgalSDo355CBPF, were confirmed by DNA sequencing.

Variant 4,6-Dehydratase Expression Constructs. All 4,6-dehydratase variants were prepared by site-directed mutagenesis of pTZ18UgalSDo355CBPF using a Stratagene QuickChange kit. Oligonucleotide primer sequences are listed in the Supporting Information. The DNA sequence was determined for the entire ORF for each variant to confirm the existence of planned modifications, and the absence of unexpected alterations.

Affinity Purification of 4,6-Dehydratase. BL21(DE3)pLysS cells (Novagen) were transformed with pTZ18UgalSDo355-CBPF and grown at 37 °C in 2×YT medium supplemented with 50 μg/mL ampicillin and 37 μg/mL chloramphenicol. Cells were induced (OD_{600} = 1.2) with 0.2% lactose, harvested by centrifugation 12 h post-induction, and frozen as pellets in liquid nitrogen. For purification, cells were thawed and resuspended to 0.33 g/mL in ice-cold lysis buffer (20 mM MOPS, pH 7.0, 200 mM NaCl, 5 mM PMSF) and broken by sonication. Following sonication, EDTA (0.5 M, sodium salt, pH 8.0) was added to a concentration of 5 mM; all subsequent steps were carried out on ice, or at 4 °C. Cell debris was removed by centrifugation (30 min, 8000 rpm, Sorvall GSA rotor). The supernatant was brought to 3% streptomycin sulfate, and the precipitate was removed by centrifugation as above. The supernatant was diluted with 1 volume of running buffer (20 mM MOPS, pH 7.0, 200 mM NaCl), and loaded directly onto a chitin affinity column (200 mL, 4 cm diameter) by gravity. The column was washed with 2 L of running buffer and then 600 mL of cleavage buffer (running buffer with 30 mM β-mercaptoethanol). Thiolysis of the intein-thioester was allowed to proceed for 12−14 h whereupon free 4,6-dehydratase was eluted from the column with running buffer. Enzyme was exchanged into 20 mM MOPS, pH 7.0, 1 mM DTT by ultrafiltration (YM-30, and Centriprep-30, Amicon) and concentrated to 10 mg/mL prior to freezing. The 4,6-dehydratase was delivered dropwise into liquid nitrogen and stored at −80 °C.

[β-^{32}P]dTDP-Glucose. Carrier-free [^{32}P]orthophosphate (250 μCi; 10 mCi/mL) and 3 mg of glycogen (washed by ultrafiltration, Microcon 10, Amicon) were converted by 1 mg of glycogen phosphorylase, and 0.1 mg of PGM, to glucose-1-[^{32}P]phosphate and glucose-6-[^{32}P]phosphate in 200 μL of 50 mM MOPS, pH 7.0, 10% glycerol, 5 mM $MgCl_2$, 1 mM DTT at 18 °C in 2 days. The resulting equilibrium mixture of glucose-1-[^{32}P]phosphate and glucose-6-[^{32}P]phosphate was ultrafiltered (Centricon 10, Amicon) to remove enzyme. The eluent was augmented with 5 mM dTTP, 0.1 mg of PGM, 25 units of UDP-glucose-pyrophosphorylase, and 0.01 mg of inorganic pyrophosphatase and diluted to 500 μL in 100 mM TRIS-HCl, pH 8.0, 10% glycerol, 10 mM $MgCl_2$, 1 mM DTT at 18 °C for 4 days. The resulting mixture containing [β-^{32}P]dTDP-glucose was purified by HPLC reverse-phase chromatography (Waters, Nova Pak C_{18}, in 100 mM potassium phosphate, pH 6.0, isocratic), and then anion exchange chromatography (Pharmacia, 5 mL Mono-Q, 10−500 mM NH_4OAc, 50 mL gradient), and again to reverse-phase chromatography (same column, run with water). [β-^{32}P]dTDP-glucose was detected as a single radioactive spot by TLC (described below, R_f = 0.3). The synthesis was performed in two steps to prevent radioisotopic dilution of [^{32}P]P_i by cold phosphate generated by the hydrolysis of pyrophosphate from the deoxythymidylylation reaction.

[β-^{32}P]dTDP-Glucose and [β-^{32}P]dTDP-Glucose-d_7 for Isotope Effects. For the measurement of isotope effects, [β-^{32}P]dTDP-glucose and [β-^{32}P]dTDP-glucose-d_7 were synthesized and purified in parallel. Then 1 mM glucose (or [1,2,3,4,5,6,6-$^2H_7$]glucose), 0.5 mCi of [γ-^{32}P]ATP, and 1 mM dTTP were converted by 1 unit of hexokinase, 0.01 unit of PGM, 1.3 units of UDP-glucose-pyrophosphorylase, and 0.01 unit of inorganic pyrophosphatase in 100 μL of 100 mM potassium phosphate, pH 7.8, 10% glycerol, 5 mM $MgCl_2$, and 1 mM DTT, at 4 °C, to [β-^{32}P]dTDP-glucose (or [β-^{32}P]dTDP-glucose-d_7) and P_i in 6 days. The labeled dTDP-glucoses were subjected to anion exchange chromatography (Mono-Q) as described above, and were desalted by gel filtration (TOSOHAAS, Toyopearl HW-40S, 120 mL, in water).

dTDP-6-Deoxyglucose/galactose. dTDP-4-Keto-6-deoxyglucose was synthesized enzymatically from dTDP-glucose using 4,6-dehydratase. The dTDP-4-keto-6-deoxyglucose was ultrafiltered (Centricon 10, Amicon) to remove enzyme. The filtrate was treated with 50 mM sodium borohydride in 200 mM potassium bicinate, pH 8.5, until dTDP-4-keto-6-deoxyglucose was no longer detected (*14*). The nonstereospecific reduction of the 4-keto functionality resulted in a mixture of gluco- and galacto-dTDP-6-deoxypyranoses. The mixture of dTDP-6-deoxypyranoses was desalted on a Toyopearl HW-40S gel filtration column (2.6 × 40 cm) equilibrated and eluted with water.

Circular Dichroism Spectra. Samples of wt 4,6-dehydratase prepared using either the chitin/intein fusion construct

or the nonfusion expression system, and each variant 4,6-dehydratase, were exchanged into 50 mM pH 7.5 potassium phosphate using Sephadex G50 spin columns. Sample concentrations were adjusted to 0.2−0.4 A_{280} unit/mL, and their circular dichroism spectra were recorded from 185 to 300 nm using an Aviv 62A DS Circular Dichroism Spectrometer. Molar ellipticity spectra were identical within error.

Dehydratase Assay and Steady-State Kinetics. Aliquots of the reaction (37 °C in 100 mM TRIS, pH 7.5, 1 mM DTT, 1 mM EDTA) were quenched at various times by addition to a silica gel TLC plate (Whatman, LK6DF silica gel 60 A). Plates were dried and then developed in 30% methanol, 5% acetic acid, 2% triethylamine, in ethanol. Initial rates for the steady-state conversion of substrate to product were determined by quantitation of [β-^{32}P]dTDP-glucose (R_f = 0.3) and [β-^{32}P]dTDP-4-keto-6-deoxyglucose (R_f = 0.4) by phosphoimagery (Molecular Dynamics). Steady-state kinetic characterization of wt and variants was performed in triplicate at substrate concentrations bracketing the Michaelis constant. Final kinetic constants were determined using a nonlinear regression to fit the data of rate vs substrate concentration to the Michaelis−Menten equation.

Buffer System for pH Studies. A 0.08 M piperazine (pK_As = 5.3 and 9.7), 0.1 M HEPES (pK_A = 7.5) solution was used to buffer reactions across the required range of pH values. Buffers were prepared by titrating the solution to the desired pH, then by adjusting the ionic strength to 0.4 mM with potassium chloride (*15*). No significant buffer concentration dependence was observed when 4,6-dehydratase was assayed at several buffer concentrations. Precise pH values for each buffer solution were measured at 16 °C.

Measuring Active Site Proton Release upon Addition of dTDP-Xylose. All pH measurements were made at 16 °C, under a blanket of argon gas, with magnetic stirring using a Corning semi-micro combination #476156 pH probe. Unbuffered stock solutions of wt 4,6-dehydratase and dTDP-xylose were carefully adjusted to pH 8.2. The stock concentrations were 0.385 and 4.45 mM, respectively, after titration. The pH of 1.5 mL (578 μmol) of enzyme stock was monitored as 0.136 mL (1.05 equiv) of the dTDP-xylose stock was added. Measured pH values dropped to 8.13, and the amount of NaOH needed to bring the pH back to 8.2 was 0.14 mmol, accounting for 24% of enzyme active sites. Under these conditions, 65% of wt active sites contain NADH as determined spectrophotometrically. Only 37% of the expected proton yield is accounted for in this experiment, which supports the retention of most, if not all, of the protons generated during ketonization of dTDP-xylose in the enzyme active site. The substoichiometric release of protons may be due to the binding of the anionic nucleotide-sugar.

Amino Acid Sequence Alignments Used for Model. Multiple amino acid sequence alignments of six bacterial 4-epimerases and nine bacterial 4,6-dehydratases were generated using CLUSTAL W (*16*). The 4-epimerase sequences are from the following organisms/protein accession numbers: *E. coli*/CAA29573; *Erwinia amylovora*/CAA53767; *Haemophillus influenza*/CAA40567; *Neisseria gonorrheae*/CAA79721; *Neisseria meningitidis*/AAA63156; and *Salmonella enterica*/CAA58779. The 4,6-dehydratase sequences are from the following organisms/protein accession numbers: *E. coli* (strain *K-12*) RfbB/AAB88398; *E. coli* (strain *K-12*) RffG/AAC76793; *Neisseria gonorrheae*/CAA83652; *Neisseria meningitidis*/AAA63157; *Saccharopolyspora erythraea*/AAA68211; *Salmonella enterica* RfbB/CAA40115; *Shigella flexneri* RfbB/AAA53679; *Streptomyces fradiae*/U08223; *Streptomyces griseus*/CAA44444. Twenty-six additional 4,6-dehydratase amino acid sequences were aligned after generating the homology model. That sequence alignment was generated using the following additional organisms/protein accession numbers: *Acetobacter xylinus*/CAC12984; *Actinobacillus actinomycetemcommitans*/T00102; *Actinoplanes sp.*/CAA77209; *Aeropyrum pernix*/BAA80166; *Archaeoglobus fulgidus*/D69290; *Campylobacter jejuni*/CAC01395; *Haemophillus influenza*/AAC22531; *Methanobacterium thermoautotrophicum*/H69105; *Mycobacterium tuberculosis*/CAB08730; *Pyrococcus abyssi*/B75098; *Pyrococcus horikoshii*/BAA29500; *Rhizobium sp. NGR234*/AAB91680; *Sinorhizobium mililoti*/CAB01951; *Streptococcus mutans*/BAA11249; *Streptococcus pneumoniae*/CAB05932; *Streptomyces argillaceus*/CAA07755; *Streptomyces avermitilis*/BAA84593; *Streptomyces coelicolor* A3(2)/CAB61555; *Streptomyces rimosus*/AAD31893; *Streptomyces spheroides*/AAF67513; *Streptomyces tenebrarius*/AAG18457; *Streptomyces violaceruber*/S58686; *Sulfolobus solfataricus*/CAB57474; *Synechocystis sp.*/BAA10518; *Xanthomonas campestris*/AAA16192; and *Xylella fastidiosa*/AAF83068. Many of the above amino acid sequences were identified by their sequence similarity to known 4,6-dehydratase sequences and have not been verified biochemically. Additional support for their assignment may be gleaned from genetic context, as many of the genes were found in biosynthetic operons involved in the production of 6-deoxysugar-containing products.

RESULTS

Affinity Purification of 4,6-Dehydratase and Comparison to Previously Purified Enzyme. To ensure purification of recombinant 4,6-dehydratase variants from contaminating host genomic background wt 4,6-dehydratase (RffG and/or RfbB), we employed the IMPACT Protein Purification System (New England Biolabs). 4,6-Dehydratase is expressed as a fusion protein connected to a chitin binding protein through a self-cleaving intein linkage. The fusion protein binds to a column of immobilized chitin, allowing other proteins to be washed away. The 4,6-dehydratase is released by thiol-induced auto-cleavage of the intein, and washed from the column in its native state. Samples of wt 4,6-dehydratase purified by the affinity method and by our previously published nonaffinity method were indistinguishable by steady-state kinetic assays and circular dichroism spectroscopy. Both batches of 4,6-dehydratase have a full complement of tightly bound NAD^+ as determined by chemical reduction of NAD^+ to NADH using dimethylamine borane complex and by quantifying NADH and protein using previously reported extinction coefficients (*7*).

Steady-State Kinetic Parameters for 4,6-Dehydratase. The spectrophotometric 4,6-dehydratase assay (*14*) was not sensitive enough to accurately measure K_M values (*7*). A radiochemical assay that uses a modified thin-layer chromatography system from Stein et al. (*17*) to separate dTDP-glucose from dTDP-4-keto-6-deoxyglucose was developed. Steady-state kinetic parameters for wt enzyme with dTDP-glucose and UDP-glucose are listed in Table 1 along with K_I values for dTDP-galactose and dTDP-xylose. No conver-

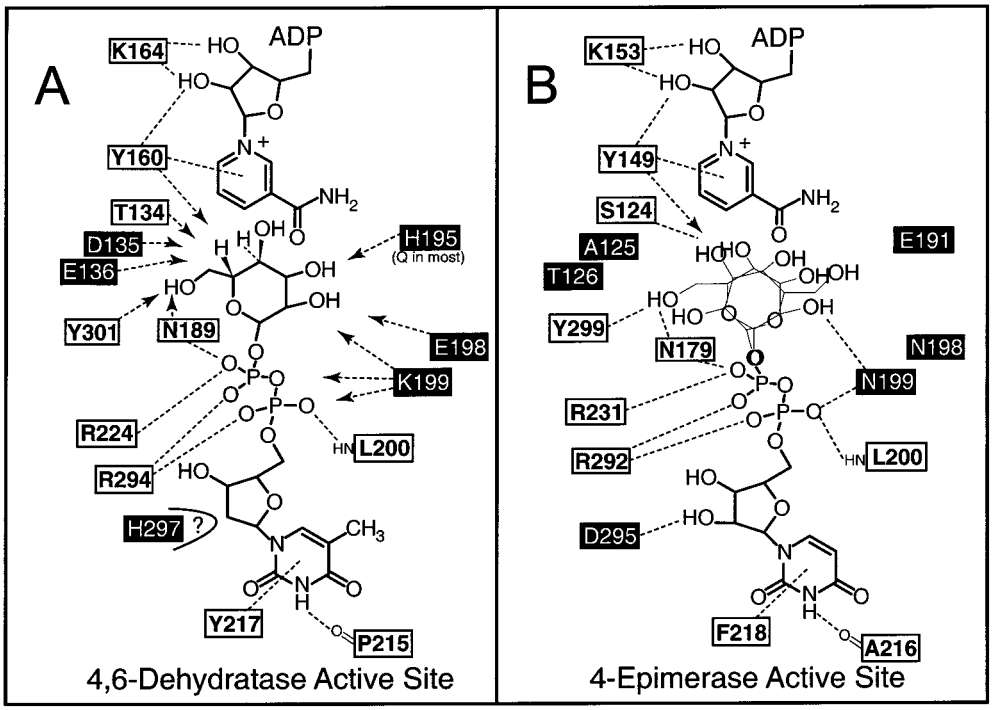

FIGURE 1: Active site models of 4,6-dehydratase and 4-epimerase. Panels A and B are schematic representations of the active sites of 4,6-dehydratase and 4-epimerase, respectively. Panel B shows the two pyranose active site conformations, illustrating the mechanism for nonstereospecific hydride transfer in 4-epimerase. Residues that are conserved in both enzymes are indicated with black characters in white boxes; residues that are conserved in each enzyme, but differ from 4,6-dehydratase to 4-epimerase, are indicated by white characters in black boxes. Enzyme−NAD^+ or enzyme−substrate-nucleotide interactions conserved in both 4-epimerase and 4,6-dehydratase are shown as dashed lines, and potential interactions with dashed arrows.

Table 1: Steady-State Kinetic Parameters for Wt 4,6-Dehydratase with Natural Substrate and Analogues[a]

RffG	k_{cat} (s^{-1})	k_{cat}/K_M ($mM^{-1}\cdot s^{-1}$)	K_M (mM)	K_I (mM)
dTDP-glucose	4.9 (±0.2)	820 (±60)	0.0060 (±0.0007)	–
UDP-glucose[b]	0.024 (±0.002)	0.00079 (±0.00007)	30 (±4)	–
dTDP-galactose	no turnover detected[b,c]			0.097 (±0.007)
dTDP-xylose	no turnover detected[d]			0.0112 (±0.0007)

[a] Parameters were determined at 37 °C in 100 mM TRIS-HCl, pH 7.5, 1 mM DTT unless otherwise noted. [b] Product formation was assayed by the Okazaki method (*14*). [c] A mixture containing 1 mM dTDP-galactose, 77 μM 4,6-dehydratase, 100 mM TRIS-HCl, pH 7.5, and 1 mM DTT was incubated at 19 °C for 16 h. [d] dTDP-Xylose cannot be converted to product as it lacks the C6 -CH_2OH (see Scheme 4).

sion of 1 mM dTDP-galactose to dTDP-4-keto-6-deoxyglucose was detected after 16 h with 77 μM 4,6-dehydratase at 19 °C. dTDP-Galactose inhibited turnover of dTDP-glucose by 4,6-dehydratase with a K_I of 97 μM. Clearly dTDP-galactose binds, but cannot be oxidized to the common dTDP-4-ketoglucose intermediate. This provides important information about the mode of pyranose binding in 4,6-dehydratase. Clearly the 4,6-dehydratase does not allow the same degree of pyranose conformational motility that is required for catalysis in the homologous 4-epimerase.

Active Site Model. The structural and mechanistic similarities between 4-epimerase and 4,6-dehydratase were used to assemble an active site model for 4,6-dehydratase based upon the 3-dimensional structure of the 4-epimerase/NADH abortive complex with UDP-glucose (PDB 1XEL, *18*). To this structure we assigned the approximate positions of 4,6-dehydratase residues to the C_α positions of the corresponding epimerase residues identified from the aligned amino acid sequences (details are discussed under *Methods*). Schematic active site representations of both 4,6-dehydratase and 4-epimerase are shown in Figure 1 A,B. The position of the pyranose moiety in the 4,6-dehydratase model was constrained by the requirement for hydride transfer from glucosyl C4 to nicotinamide C4. The 4,6-dehydratase will not allow the same degree of motility for the bound glucosyl moiety previously demonstrated in 4-epimerase. This assumption is supported by the complete absence of turnover observed with dTDP-galactose. The model's substrate placement also allows reasonable access of the nicotinamide to glucosyl C6 of the dTDP-4-keto-glucose-5,6-ene intermediate for the hydride attack *anti* to re-addition of the C5 proton in the final chemical step of the mechanism.

A partially refined 3-dimensional structure of 4,6-dehydratase holoenzyme (with bound NAD^+ but no substrate, PDB 1BXK) confirms the similar overall chain folds of 4-epimerase and 4,6-dehydratase. A loop from $Arg294^{DEH}$ to $Arg300^{DEH}$ of the deoxythymidine-5′-diphosphate binding subsite is missing from the 3-dimensional structural model, so it is not possible to confirm residue placement for one side of the nucleotide-sugar binding pocket. Figure 2 is a stereoview showing the 4,6-dehydratase residues from Figure 1A that were included in the X-ray crystallographic model. The position of $Tyr301^{DEH}$ may be considerably different in a substrate−nucleotide complex than from what is shown in Figure 2, as it is the first resolved residue following a missing loop in the crystal structure model. While the approximate placement of residues in our model is confirmed, little additional information about specific interactions can be gleaned from the structure in the absence of substrate.

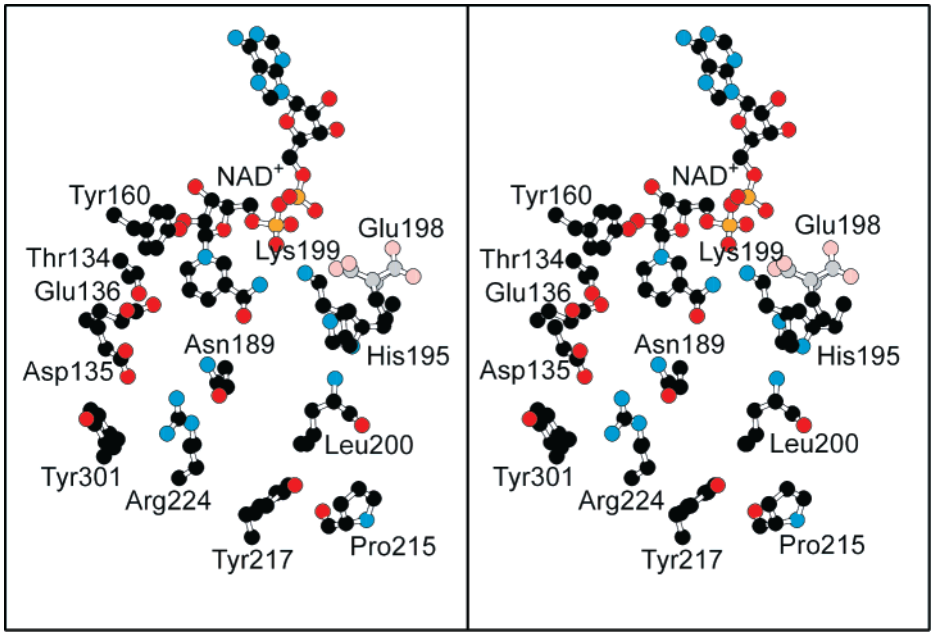

FIGURE 2: Active site structure of 4,6-dehydratase NAD^+ lacking substrate-nucleotide. Stereoview from a partially refined structure of 4,6-dehydratase showing the positions of resolved residues that may be involved in enzyme−substrate interactions. The precise orientation of the $Glu198^{DEH}$ side chain is not defined; two configurations are represented using gray carbon atoms and salmon oxygen atoms. The figure was constructed from the PDF file 1BXK using MolView (*29*).

Table 2: Steady-State Kinetic Parameters for 4,6-Dehydratase Active Site Variants

4,6-dehydratase	k_{cat} (s^{-1})	$-\Delta^a$	k_{cat}/K_M ($mM^{-1}\cdot s^{-1}$)	$-\Delta$	K_M (mM)	$+\Delta^a$
D135N	0.0395 (±0.0009)	124	5.0 (±0.2)	164	0.0079 (±0.0009)	1.3
D135A	0.022 (±0.002)	223	3.0 (±0.5)	273	0.007 (±0.002)	1.2
E136Q	0.073 (±0.006)	67	7 (±1)	117	0.009 (±0.002)	1.5
E136A	0.017 (±0.001)	288	1.4 (±0.2)	586	0.012 (±0.002)	2
D135N/E136Q	0.024 (±0.005)	204	1.3 (±0.3)	631	0.019 (±0.007)	3.2
E198Q	0.019 (±0.001)	258	1.6 (±0.2)	513	0.011 (±0.002)	1.8
K199M	0.0425 (±0.0007)	115	5.3 (±0.3)	146	0.0080 (±0.0006)	1.3
K199R	0.017 (±0.001)	288	1.3 (±0.2)	631	0.013 (±0.003)	2.2
Y301F	0.042 (±0.002)	117	1.4 (±0.1)	586	0.031 (±0.004)	5.2
C187S	1.2 (±0.06)	4.1	800 (±200)	1	0.0015 (±0.0004)	0.25
C187A	0.52 (±0.04)	9.4	500 (±100)	1.6	0.0010 (±0.0002)	0.17
N190D	0.0111 (±0.0007)	441	0.44 (±0.08)	1860	0.025 (±0.004)	4.2
N190H	0.0226 (±0.0004)	217	3.1 (±0.2)	265	0.0073 (±0.0004)	1.2
N190A	0.0089 (±0.0006)	551	1.6 (±0.3)	513	0.0055 (±0.0009)	0.92
H232Q	0.043 (±0.004)	114	6 (±2)	137	0.008 (±0.002)	1.3
H232N	0.72 (±0.08)	6.8	150 (±60)	5.5	0.005 (±0.002)	0.83
H232A	0.085 (±0.004)	58	26 (±4)	32	0.0033 (±0.0005)	0.55

[a] ±Δ column heading refers to the *x*-fold change in the parameter with respect to wt, given in Table 1.

Identification of Residues Important for Catalysis. Mutation of 4,6-dehydratase active site residues was undertaken in order to investigate their roles in catalysis. Residues were divided into two groups, the first of which consisted of one or more of the following: $Asp135^{DEH}$; $Glu136^{DEH}$; $Glu198^{DEH}$; $Lys199^{DEH}$; and $Tyr301^{DEH}$. These are positioned near the glucopyranose in our model, and are conserved in all of the 35 4,6-dehydratase sequences aligned. Interestingly, these residues, with the exception of $Tyr301^{DEH}$, differ from equally well-conserved 4-epimerase residues that occupy homologous positions. Residues within this group are potentially involved in catalyzing the two steps in the 4,6-dehydratase mechanism absent in 4-epimerase, specifically the dehydration of the dTDP-4-ketoglucose intermediate and the reduction of the dTDP-4-ketoglucose-5,6-ene intermediate (Scheme 1). $Tyr301^{DEH}$ was also included in this group because of its possible hydrogen-bonding interaction with the glucosyl -6(OH). Control of C5−C6 rotational freedom will be important in directing *syn* water elimination (*19*). $His195^{DEH}$ was not included in this group because it is not conserved. The following variants have been generated: $D135N^{DEH}$; $D135A^{DEH}$; $E136Q^{DEH}$; $E136A^{DEH}$; $E198Q^{DEH}$; $K199R^{DEH}$; $K199M^{DEH}$; $Y301F^{DEH}$; and double variant $D135N/E136Q^{DEH}$. Alterations where possible were designed to introduce conservative changes that would have minimal impact on local interactions, while removing that residue's potential for performing general acid/base catalysis.

Steady-state kinetic parameters at pH 7.5 and 37 °C were measured for each variant and are listed in the upper panel of Table 2. Each member of this first group displays significantly less catalytic efficiency than wt (more than 100-fold lower k_{cat}/K_M). It is clear that all of the residues tested are important for catalysis. While no single variant displays the 4 or 5 orders of impairment in activity typically attributed

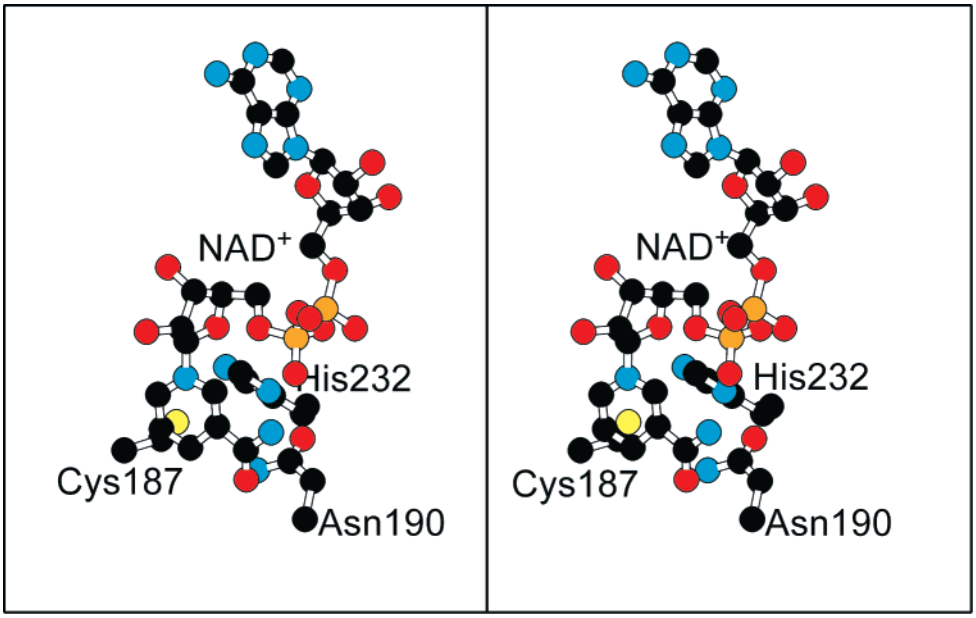

FIGURE 3: 4,6-Dehydratase *re* face nicotinamide binding pocket. Stereoview from the partially refined structure of 4,6-dehydratase showing NAD^+ and the cysteine-protease-like triad of asparagine, histidine, and cysteine residues on the *re* face of the nicotinamide ring. The figure was constructed from the PDF file 1BXK using MolView (*29*).

Table 3: Steady-State Kinetic Parameters and Isotope Effects for Wt 4,6-Dehydratase at 18 °C

	dTDP-glucose	dTDP-glucose-d_7
k_{cat} (s^{-1})	1.9 (±0.1)	0.46 (±0.02)
k_{cat}/K_M ($mM^{-1}\cdot s^{-1}$)	850 (±120)	420 (±50)
K_M (mM)	2.2 (±0.4)	1.1 (±0.2)
$^Dk_{cat}$	4.1 (±0.3)	
$^D(k_{cat}/K_M)$	2.0 (±0.4)	
^DK_M	2.0 (±0.5)	

to the deletion of a residue involved in general acid/base catalysis, the loss may be partially masked by other steps' contributions to rate limitation. Isotope effects on k_{cat} and k_{cat}/K_M for dTDP-glucose-d_7, at 18 °C, listed in Table 3, show that chemistry (one or more steps) is at least partially rate-limiting in wt. A pre-steady-state, single-turnover characterization of wt enzyme performed previously in this laboratory (dTDP-glucose-d_7, 18 °C, pH 7.5) indicates that the reduction of the glucose-5,6-ene intermediate is the major chemical step contributing to overall rate limitation (*7*). The initial ketonization chemistry occurs at a slightly faster rate, and will also contribute significantly; water elimination is apparently much faster than both of these steps.

Nicotinamide Pocket. The second group of residues selected for mutagenesis consists of $Cys187^{DEH}$, $His232^{DEH}$, and $Asn190^{DEH}$. These residues form the *re* face nicotinamide binding pocket, with hydride transfer occurring from the *si* face (Figure 3). The motif is reminiscent of the catalytic triad in papain, which functions to maintain the cysteine as a thiolate anion for nucleophilic catalysis of peptide bond hydrolysis (*20*). The presence of a thiolate anion in such close proximity to the nicotinamide ring could effect the oxidoreductive properties of the NAD^+ cofactor. This is particularly interesting in enzymes such as 4-epimerase and 4,6-dehydratase that use NAD^+ as a cofactor, as thermodynamic alterations to the cofactor's solution-state chemistry might be critical for promoting catalysis.

The following variants in this group have been generated: $C187A^{DEH}$; $C187S^{DEH}$; $N190D^{DEH}$; $N190H^{DEH}$; $N190A^{DEH}$; $H232Q^{DEH}$; $H232N^{DEH}$; and $H232A^{DEH}$, and their steady-state parameters (measured at pH 7.5 and 37 °C) are listed in the lower half of Table 2. Several conclusions can be made from these data. First, the activities of all of the $Asn190^{DEH}$ variants are seriously compromised. Second, while $H232Q^{DEH}$ and $H232A^{DEH}$ show a significant loss of activity, $C187A^{DEH}$, $C187S^{DEH}$, and $H232N^{DEH}$ do not. From these results, it is clear that $Cys187^{DEH}$ has no significant role in catalysis. The activity loss associated with $His232^{DEH}$ is residue-specific. $H232N^{DEH}$ retains activity while the alanine and glutamine variants of that residue clearly do not. There is universally no significant effect on K_M.

At the time the homology model was originally constructed, all three residues were completely conserved. Subsequently, 25 additional 4,6-dehydratase sequences have been described which support all of our conserved 4,6-dehydratase residue claims for both groups of residues except $Cys187^{DEH}$ and $His232^{DEH}$. Two sequences, from *Haemophillus influenza* and *Acetobacter xylinus*, have a serine and a threonine, respectively, at the position homologous to $Cys187^{DEH}$. In addition, two hyperthermophilic archaea, *Aeropyrum pernix* and *Sulfolobus solfataricus*, contain proline and threonine, respectively, in place of $Cys187^{DEH}$ and $His232^{DEH}$. One might easily dismiss the observed changes in the archaeal proteins as relating to the hyperthermophilicity of the organisms. Still, it is questionable, given the changes observed in the two bacterial species, whether $Cys187^{DEH}$ plays a critical part in the 4,6-dehydratase reaction in any role that cannot also be accomplished by serine or threonine. This would exclude the possibility of this motif functioning, like that of papain, to maintain a cysteineyl thiolate anion, but leaves open questions concerning the role and relevance of these residues to catalysis.

Structural Integrity of Variants. None of the active site modifications appear to cause gross structural changes. The total dinucleotide content for each variant was confirmed

spectrophotometrically by treating a sample of each variant with dimethylamine−borane complex and quantifying NADH. Except for N190D^{DEH} and H232Q^{DEH}, all of the variants appear to contain a full complement of dinucleotide. These two partially occupied variants are still largely intact, with 60% and 70% dinucleotide, respectively. In either case, the dinucleotide content did not increase with addition of exogenous NAD^+. Significant turnover was detectable for all of the 4,6-dehydratase variants, suggesting that at least some of the variants are capable of forming functional active sites. To eliminate the possibility that a minority of fully active enzyme molecules is responsible for the observed activity, CD spectra were determined for all of the variants. In each case, they were indistinguishable from wt CD spectra. CD is not sensitive to subtle structural changes that may result from amino acid alteration, but can be used to exclude extensive changes in secondary structural content that might indicate that a large fraction of the protein is incorrectly folded.

Absorption spectra for several of the purified variant 4,6-dehydratase species showed a broad, low-intensity spectral feature at 355 nm that decreased upon addition of dTDP-4-keto-6-deoxyglucose. These data are consistent with 5−30% of the enzyme containing tightly bound NADH rather than NAD^+. In variant C187A^{DEH}, over 60% of the tightly bound dinucleotide was NADH, while N190A^{DEH} had 25% NADH. Variants of Glu136^{DEH} typically also had high percentages of NADH (20−30%) while Glu198^{DEH}, Lys199^{DEH}, and His232^{DEH} variants had no tightly bound NADH. In each case where NADH was found, 4,6-dehydratase variants were treated in bulk with excess dTDP-4-keto-6-deoxyglucose to convert bound NADH back to NAD^+; enzymes thus treated were desalted to remove dTDP-sugars and exchanged into appropriate buffers supplemented with 1 mM DTT before they were used for all other experiments.

Fraction of NADH during Steady-State Turnover with dTDP-Glucose. Enzyme-bound NADH can be measured spectrophotometrically by its absorbance at 355 nm. Thus, during steady-state turnover, the fraction of enzyme−NADH can be quantified. This fraction represents the sum of the dTDP-4-ketoglucose and dTDP-4-ketoglucose-5,6-ene intermediates that exist during the steady state. We measured the percentage of the enzyme containing NADH during steady-state turnover for each variant by adding a large excess of dTDP-glucose (100−10 000-fold excess depending on activity) to the enzyme. For variants that accumulated NADH during turnover, a sharp increase in absorbance at 355 nm was observed immediately after the addition of substrate, followed by a plateau phase and recovery. The percentage values were calculated using the difference between the initial A_{355} values and the plateau at pH 7.5 and 16 °C, and are listed in Table 4.

All variants had lower steady-state NADH levels than wt, which contained 45%. Only two variants, D135A^{DEH} and Y301F^{DEH}, had steady-state levels close to wt, with 30% and 39%, respectively. Y301F^{DEH} is also unique because the λ_{MAX} for enzyme-bound NADH is red-shifted 15 nm to 370 nm; this red-shift is not observed when Y301F^{DEH} is reduced with dimethylamine−borane. Most variants have single-digit NADH percentages, while five variants, E198Q^{DEH}, N190A^{DEH}, N190D^{DEH}, H232Q^{DEH}, and the double variant D135N/E136Q^{DEH}, were below the threshold of detection with less than 0.5%.

Table 4: Percent NADH Observed in Wt and Variant RffGs with an Excess of dTDP-Glucose

4,6-dehydratase	% NADH with saturating dTDP-glucose
wt	45
D135N	9
D135A	30
E136Q	3
D135N/E136Q	<0.5
E198Q	<0.5
K199M	2
K199R	2
Y301F	39
C187S	5
C187A	8
N190D	<0.5
N190A	<0.5
H232Q	<0.5
H232N	3

Scheme 3

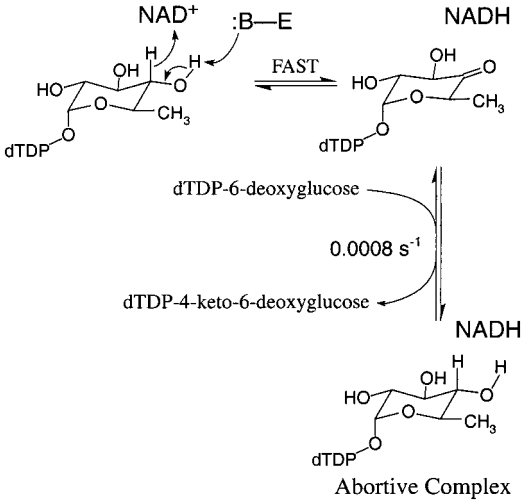

Initial Dehydration Step: dTDP-6-Deoxyglucose and dTDP-Xylose. Experiments have been described in the literature using a substrate analogue, dTDP-6-deoxyglucose, that is unable to eliminate water (*9*). In our hands, treatment of 4,6-dehydratase with dTDP-6-deoxyglucose resulted in the slow (0.0008 s^{-1}) formation of abortive complex(Scheme 3) that complicates the analysis of the magnitude of the initial redox step (7−8% active sites with saturating dTDP-6-deoxyglucose). As an alternative to dTDP-6-deoxyglucose, dTDP-xylose was synthesized to probe the first step in the 4,6-dehydratase reaction. The initial redox chemistry can be accomplished as depicted in Scheme 4, to produce a dTDP-4-ketoxylose species. Interestingly, treatment of 4,6-dehydratase with dTDP-xylose does not appear to result in the formation of an abortive complex. dTDP-Xylose rapidly produces a stable, broad spectral feature centered at 355 nm that is identical to that observed previously in spectra of the 4,6-dehydratase/NADH complex. Formation of this complex is reversible as demonstrated by disappearance of the 355 nm chromophore through multiple rounds of dilution and ultrafiltration. A solution containing 0.05 mM dTDP-xylose and 0.025 mM 4,6-dehydratase at equilibrium was denatured in 2% trichloroacetic acid, the denatured protein was removed

Scheme 4

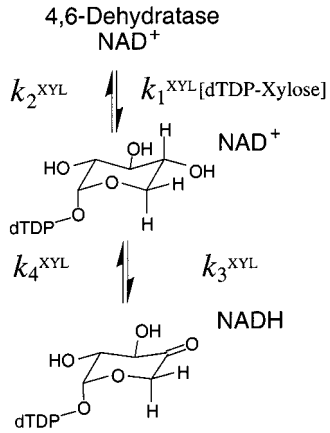

by centrifugation, and the supernatant was analyzed by ion-paired reverse-phase HPLC. dTDP-Xylose was observed with a retention time of 12.4 min. An additional peak with a 267 nm λ_{MAX} absorption spectrum was observed at a retention time of 11.9 min, which upon treatment with sodium borohydride decreased in area with a concomitant increase in the dTDP-xylose peak area. Treatment of part of the quenched sample with sodium borotritiide followed by HPLC analysis and quantitation of radioactivity showed that significant radioactivity emerged with the dTDP-xylose peak. A similar mixture of dTDP-xylose and 4,6-dehydratase was denatured in 65 °C ethanol and analyzed by MALDI-TOF in the negative ion mode using previously described techniques (*7*). Peaks at masses corresponding to both dTDP-xylose and dTDP-ketoxylose (neutral mass −1) were detected at *m*/*z* 533.2 and 531.2, respectively. These data support the reversible formation of dTDP-ketoxylose coincident with NADH as depicted in Scheme 4.

dTDP-Xylose Binding and Reaction. It was not possible to determine the apparent dissociation constant for dTDP-xylose spectrophotometrically following NADH production because the value was low enough that accurate quantitation of enzyme-bound NADH at suitable enzyme concentrations ($<K_D^{XYL}$) became impossible. However, dTDP-xylose does inhibit turnover of dTDP-glucose by 4,6-dehydratase with a K_I^{XYL} of 11.2 μM (Table 1). This K_I^{XYL} term is necessarily a combination of all four rate constants shown in Scheme 4, and does not simply reflect the rates constants (k_1^{XYL}[dTDP-xylose] and k_2^{XYL}) across the binding and release step.

Saturation of 4,6-dehydratase with dTDP-xylose results in reduction of 73% of the tightly bound NAD^+ to NADH. Under saturating conditions, the second-order rate constant k_1^{XYL}[dTDP-xylose] (Scheme 4) becomes very large so that all of the enzyme exists with bound nucleotide-sugar, and only the k_3^{XYL} and k_4^{XYL} terms affect the relative amounts of NAD^+/dTDP-xylose and NADH/dTDP-ketoxylose observed at equilibrium. The spectrophotometrically observed fraction of NADH with saturating dTDP-xylose is $k_3^{XYL}/(k_3^{XYL} + k_4^{XYL})$ at equilibrium. That quantity was measured over a pH range for the following variants: $D135N^{DEH}$; $D135A^{DEH}$; $E136Q^{DEH}$; $E136A^{DEH}$; $E198Q^{DEH}$; $K199R^{DEH}$; $K199M^{DEH}$; $Y301F^{DEH}$; $C187A^{DEH}$; $C187S^{DEH}$; $N190D^{DEH}$; $N190A^{DEH}$; $H232Q^{DEH}$; and $H232N^{DEH}$; and the double variant $D135N/E136Q^{DEH}$. The pH profiles generated from those measurements at 16 °C are shown in Figure 4.

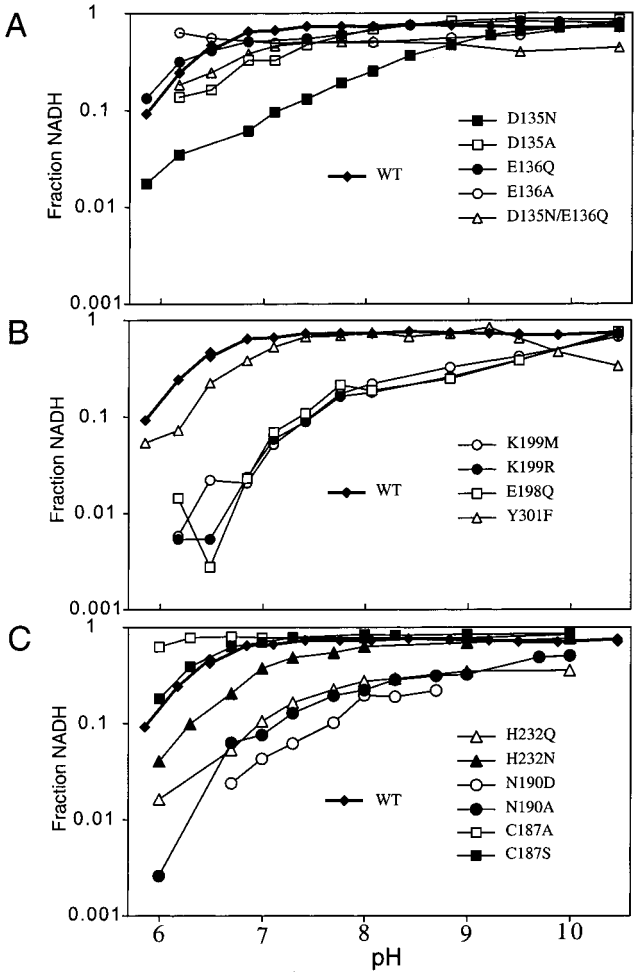

FIGURE 4: Equilibrium fraction of NADH with saturating dTDP-xylose over a range of pH. Panels A−C show the pH dependence of the fraction of NADH of the total enzyme dinucleotide content measured with saturating dTDP-xylose. A key is included in each panel, as are wt profiles for comparison.

The pH dependence of $k_3^{XYL}/(k_3^{XYL} + k_4^{XYL})$ when wt 4,6-dehydratase is saturated with dTDP-xylose is shown for comparison in all three panels (A, B, and C) in Figure 4. The curve shows a 70−80% NADH plateau from pH 10.5 to 7.5, which drops off to 10% NADH as the pH decreases to below 6.0. While it is clear that the NAD^+-dependent oxidation of dTDP-xylose to NADH and dTDP-ketoxylose will generate a proton, it is not obvious whether that proton will be released from the active site to solution. This proton release would directly link the pH of the solution to the fraction of NADH observed; alkaline conditions would pull the equilibrium toward NADH and dTDP-ketoxylose, while acidic conditions would pull the equilibrium toward NAD^+ and bound dTDP-xylose. Attempts to directly measure proton release upon addition of dTDP-xylose to concentrated stocks of unbuffered wt 4,6-dehydratase resulted in a fraction of the expected drop in pH for the observed percentage of NADH formed. The pH dependence of the equilibrium in the NAD^+-dependent oxidation of dTDP-xylose appears to be due to changes in protonation state within the 4,6-dehydratase active site.

The rate of approach to equilibrium with saturating dTDP-xylose is equal to the sum of k_3^{XYL} and k_4^{XYL}. That quantity was measured either by stopped-flow or by standard spectrophotometry at pH 7.5 and 16 °C for all of the variants

Table 5: Rate Constants for the Reaction of 4,6-Dehydratase with Saturating dTDP-Xylose

4,6-dehydratase	rate of approach to equilibrium, $k_3^{XYL} + k_4^{XYL}$ (s^{-1})	fraction NADH at equilibrium, $k_3^{XYL}/(k_3^{XYL} + k_4^{XYL})$	k_3^{XYL} (s^{-1})	k_4^{XYL}(s^{-1}) (fold Δ from wt)		(fold Δ from wt)
wt	1.4	0.73	1	(1)	0.4	(1)
D135N	0.6	0.18	0.1	(10)	0.5	(0.8)
D135A	0.32	0.57	0.2	(5)	0.1	(4)
E136Q	1	0.55	0.6	(1.67)	0.4	(1)
E136A	0.54	0.47	0.3	(3.33)	0.3	(1.33)
D135N/E136Q	0.13	0.5	0.07	(14.3)	0.07	(5.7)
E198Q	0.00028	0.22	0.00006	(16,700)	0.0002	(2000)
K199M	0.00012	0.17	0.00002	(50000)	0.0001	(4000)
K199R	0.0011	0.16	0.0002	(5000)	0.0009	(440)
Y301F	1.6	0.68	1.1	(0.91)	0.5	(0.8)
C187S	0.53	0.84	0.45	(2.2)	0.085	(4.7)
C187A	0.23	0.78	0.18	(5.6)	0.051	(7.9)
N190D	0.067	0.102	0.0068	(146)	0.060	(6.6)
N190A	0.21	0.195	0.041	(24.4)	0.17	(2.4)
H232Q	1.4	0.52	0.74	(1.4)	0.68	(0.6)
H232N	0.67	0.20	0.13	(7.7)	0.53	(0.8)

listed immediately above. The concentration of dTDP-xylose needed to saturate tens of micromolar enzyme was typically in the hundreds of micromolar range. Saturation was tested empirically by taking measurements at multiple concentrations of dTDP-xylose until dTDP-xylose concentration dependence was not observed. The fraction of NADH observed [$k_3^{XYL}/(k_3^{XYL} + k_4^{XYL})$] at pH 7.5 and 16 °C and the rate of approach to equilibrium values ($k_3^{XYL} + k_4^{XYL}$) for each variant are listed in Table 5, along with calculated values of k_3^{XYL} and k_4^{XYL}.

DISCUSSION

Catalysis of Dehydrogenation. Substrate dehydrogenation requires hydride abstraction from glucosyl C4 in concert with general base catalysis to remove the proton from the C4-(OH). This step is mechanistically identical to the first step in the 4-epimerase reaction, where previous work has implicated residues $Lys153^{EPIM}$, $Tyr149^{EPIM}$, and $Ser124^{EPIM}$ as key participants, with $Tyr149^{EPIM}$ generally held to be the active site base (*21*). The corresponding residues in 4,6-dehydratase are $Lys164^{DEH}$, $Tyr160^{DEH}$, and $Thr134^{DEH}$. The tyrosine and lysine residues are the signature motif for the extended short chain dehydrogenase/reductase superfamily (*10*), a broad group of enzymes that use NAD^+/NADH to catalyze oxidoreductase reactions. This core group of catalytic residues for hydride transfer is broadly conserved. Analysis of these residues will be reported in a forthcoming article.

Dehydration. The second chemical step, elimination of water, requires an acid at the active site to protonate the leaving hydroxyl group and a base to abstract the proton from C5. While 4-epimerase does not catalyze water elimination, the comparison of the two enzymes is important, as one would expect 4-epimerase to be deliberately devoid of residues capable of catalyzing this potential side reaction. Thus, we identified conserved active site residues in 4,6-dehydratase that were different from conserved residues at analogous positions in 4-epimerase. The primary candidate for catalyzing water elimination is $Glu136^{DEH}$, although other residues cannot be excluded. Conserved glutamate residues have been proposed to be involved in C5 proton abstraction in the *Salmonella typhimurium* dTDP-4,6-dehydratase (RmlB) and *E. coli* GDP-mannose 4,6-dehydratase systems, but no biochemical data have yet been offered that support these assignments (*3*, *22*).

Scheme 5

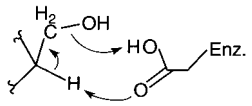

Two general mechanisms can be proposed for water elimination chemistry. Separate residues may deprotonate C5 and protonate the leaving C6(OH). Alternatively, as depicted in Scheme 5, a single glutamic acid residue might accomplish both types of catalysis simultaneously. The latter mechanism has particular appeal given the close proximity of $Glu136^{DEH}$ to C5 and C6 in the model. Also, inasmuch as the stereochemistry of water elimination is *syn* (*19*), this mechanism would secure the 6-hydroxyl in the appropriate C5−C6 bond rotational conformation.

The mechanism invoking two distinct residues to catalyze water elimination becomes more provocative if the base in the initial ketonization step functions as the acid that protonates the leaving C6-hydroxyl. There are two reasons why this arrangement is attractive. First, following a complete cycle of catalysis, all of the residues would be in the correct protonation state for the next round of catalysis. Second, if the conjugate base of that acid is an anion, it could provide an electrostatic driving force for the oxidation of the cofactor to NAD^+ with concomitant reduction of dTDP-4-keto-glucose-5,6-ene. For example, homology with the 4-epimerase supports the identification of $Tyr160^{DEH}$ as the residue involved in the general base catalysis of the first step. In the first Michaelis complex, the $Tyr160^{DEH}$ tyrosinate anion is in close proximity to the NAD^+ nicotinamide cation. Once the first redox step occurs, both the $Tyr160^{DEH}$ and the nicotinamide lose their charges as the $Tyr160^{DEH}$ becomes protonated, and the NAD^+ is reduced to NADH. If the $Tyr160^{DEH}$ were to protonate the leaving C6-hydroxyl during water elimination, negative charge would be reestablished adjacent to the nicotinamide, thus driving the final chemical step to allow re-formation of the tyrosinate−NAD^+ ion pair.

Reduction of the Glucose-5,6-ene. The final chemical step requires hydride transfer to glucosyl C6, and an acid in the

active site to protonate C5. This step may reuse residues involved in catalyzing the initial two steps. The same residue that abstracted the proton from C5 in the preceding step probably accomplishes reprotonation of C5 during glucos-5,6-ene reduction. Rapid solvent hydrogen exchange from this residue would be consistent with all of the C5 hydrogen exchange phenomena observed hence.

The hydride transfer from glucosyl C4 to NAD^+ and back to C6 might be accomplished without major changes in pyranose binding. As suggested in a recent review by Giraud and Naismith, a slight shifting of the pyranose within the active site would allow better access of the NADH for reduction of the glucose-5,6-ene intermediate (*3*). This would still allow for a more tightly bound hexopyranose moiety in 4,6-dehydratase than in 4-epimerase, where the mechanism requires torsional mobility of the sugar. Given the larger number of chemical steps in 4,6-dehydratase than 4-epimerase, it is not surprising to find the 4,6-dehydratase pyranose binding pocket more extensively functionalized.

Further 4-Epimerase Comparison. One of the most fascinating characteristics of 4-epimerase concerns the communication between the nucleotide-sugar binding site and the NAD^+ pocket. Considerable changes in cofactor reactivity are effected upon binding of UDP-sugar, UDP or UMP, which make the reduction of tightly bound NAD^+ to NADH much more facile (*23*). The 4,6-dehydratase, interestingly, does not share this property with 4-epimerase. The rates of reduction of NAD^+ by 100 mM dimethylamine−borane complex in 100 mM TRIS-HCl, pH 7.5, 2 mM EDTA, 1 mM DTT at 18 °C, with either no added nucleotide, 1 mM dTDP, or 1 mM dTMP, are 0.043, 0.021, and 0.041 min^{-1}, respectively. In these experiments, dTDP appears to be protecting NAD^+ from reduction, while dTMP shows the same rate of reduction as wt. Clearly 4,6-dehydratase has different requirements for catalysis, compared with 4-epimerase, that do not involve activation of the cofactor. This difference becomes more interesting when one considers that both $Tyr149^{EPIM}$ and $Lys153^{EPIM}$ have been implicated as being important for modulating cofactor reactivity (*21*, *24*). Both of these residues are also present in 4,6-dehydratase, although they do not appear to effect cofactor reactivity in the same way as in 4-epimerase.

The 4-epimerase catalyzes epimerization of UDP-, dUDP-, and dTDP-glucose (*25*). For the *E. coli* strain B 4,6-dehydratase, values for k_{cat} and k_{cat}/K_M of 9.1 s^{-1} and 130 000 M^{-1} s^{-1} with dTDP-glucose, and 9.1 s^{-1} and 4100 M^{-1} s^{-1} with dUDP-glucose have been reported; UDP-glucose was reported not to be a substrate (*26*). In our hands, values for k_{cat} and k_{cat}/K_M for *E. coli* RffG 4,6-dehydratase were found to be 4.9 s^{-1} and 820 000 M^{-1} s^{-1} with dTDP-glucose and 0.024 (±0.002) s^{-1} and 0.79 (±0.07) M^{-1} s^{-1} with UDP-glucose. While there is a 30-fold difference in k_{cat}/K_M between dTDP-glucose and dUDP-glucose, k_{cat} is the same. These results demonstrate the sensitivity of the second-order steady-state rate constant to the absence of the thymidyl -5(CH_3) group, while the rate of turnover is otherwise unaffected. However, the absence of the ribosyl -2(OH) is clearly much more important. An overall difference in the second-order rate constant of 6 orders of magnitude is observed between dTDP-glucose and UDP-glucose, and only 30-fold of this should be attributed to the base change. In this case, catalysis is also affected, as k_{cat} is down nearly 200-fold. It is likely that the ribosyl -2(OH) perturbs the proper alignment of elements in the active site, which implies the existence of a mechanism for discriminating against ribonucleotide substrates. In the 4-epimerase active site, $Asp295^{EPIM}$ makes contacts with the ribosyl -2(OH). At that position in the 4,6-dehydratase, $His297^{DEH}$ is nearly conserved (it is glutamate in the hyperthermophilic archaea *Aeropyrum pernix*). Identification of a histidine residue at this position raises the interesting possibility that the imidazole side chain participates in a sort of steric exclusion of ribonucleotide-sugars.

Scheme 6

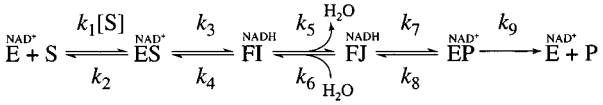

Characterization of Active Site Variants. Having observed significant drops in k_{cat} and k_{cat}/K_M for all but one of the active site residues that were modified, the task at hand becomes finding differences between these variant enzymes that allow us to assign activity loss in specific chemical steps to catalytic functions of individual residues. Unfortunately, the complexity of the 4,6-dehydratase reaction limits the interpretability of isotope effect data, which can often be useful for isolating specific steps in chemical reactions (*27*). For example, deuterium incorporated specifically at glucosyl C4 will be transferred to NAD^+, forming NADD, which will be used to reduce the dTDP-4-ketoglucose-5,6-ene intermediate, giving an observable isotope effect from a combination of the two steps. Hydrogen exchange with solvent from the C5 complicates isotope effect studies of water elimination. The fact that we observe an isotope effect on k_{cat} and k_{cat}/K_M (Table 3) demonstrates that chemistry is at least partially rate-limiting during steady-state turnover of dTDP-glucose-d_7 by wt 4,6-dehydratase.

Analysis of Steady-State NADH Levels. Steady-state NADH levels provide a quantitative measure of the accumulation of E/NADH/dTDP-4-ketoglucose (FI**)** and E/NADH/dTDP-4-ketoglucose-5,6-ene (FJ) and can be analyzed in the context of the kinetic mechanism for 4,6-dehydratase shown in Scheme 6. The fraction of NADH during the steady state can be expressed as a function of each rate constant using the net rate approximation of Cleland, by dividing the sum of the reciprocals of the net rate constants that follow NADH-containing forms (FI and FJ) by the reciprocal of the terms from the rate equation that contribute to k_{cat} (*28*). The result is a complex expression in seven rate constants. Because the reduction of the dTDP-4-ketoglucose-5,6-ene intermediate (FJ) to product (EP) is the primary contributor to overall rate limitation, and dTDP-4-ketoglucose (FI**)** does not accumulate (*7*), the expression is simplified to show that the percentage of NADH during steady-state turnover is determined by the equilibrium fraction of dTDP-glucose (ES) and dTDP-4-ketoglucose-5,6-ene [FJ; $k_3k_5/(k_4k_6 + k_3k_5)$].

We are now in a position to analyze how damage to catalysis at specific steps would change steady-state NADH levels. If deleting a critical residue significantly diminished the rate of reduction of the 4-ketoglucose-5,6-ene intermediate (k_7 and k_8), NADH levels would be unaffected. If the deletion caused a large reduction in the rate of water

elimination (k_5 and k_6), this step would become rate-limiting and the NADH levels would simplify to $k_3/(k_3 + k_4)$. Since dTDP-4-ketoglucose does not accumulate, this equilibrium apparently favors substrate. Thus, if water elimination were limiting, NADH levels would approach zero. If dehydrogenation of substrate became limiting ($k_3 + k_4$), all enzyme would be trapped in the ES complex, and NADH levels would be zero. Finally, if product release were to become limiting, the NADH level would be determined by $\{k_3k_8(k_5 + k_6)/[k_6k_8(k_3 + k_4) + k_3k_5(k_7 + k_8)]\}$, a value that reflects the equilibrium distribution across each species. Since $k_7 \gg k_8$ (*7*), the fraction of NADH will essentially be zero as most of the enzyme will be EP.

Substrate binding terms were not included in this analysis because of the assumption of saturating substrate. It is possible that in some of the variant enzymes a conformational change may follow substrate binding, thus inserting an "ES*" term into the mechanism, between ES and FI, where conversion of ES to ES* would be a first-order process. Any rate limitation contributed by the conformational change, or slowing of the conformational change in enzyme variants, would lower the percentage of NADH. No results support the occurrence of this slow conformational change or warrant the insertion of an "ES*" term into the mechanism.

dTDP-Xylose and dTDP-6-Deoxyglucose. Two nucleotide-sugars, dTDP-xylose and dTDP-6-deoxyglucose, were tested for their value in investigating substrate dehydrogenation. Like dTDP-glucose, these substrate analogues can be oxidized by 4,6-dehydratase, but they do not contain a 6-OH and thus cannot undergo water elimination. Very different behavior is observed when 4,6-dehydratase is mixed with dTDP-xylose compared with dTDP-6-deoxyglucose/galactose. dTDP-Xylose gives a rapid formation of NADH in a single phase, to 73% of the total dinucleotide. The rate of NADH formation saturates in the high hundreds of micromolar to low millimolar range and occurs at a rate of 1.4 s^{-1}. With dTDP-6-deoxyglucose/galactose, the formation of NADH is biphasic. The second phase in the dTDP-6-deoxyglucose/galactose absorbance profile likely results from formation of an abortive complex (Scheme 3); saturating dTDP-nucleotide would eventually drive the reaction to completion with 100% NADH. The first phase had a magnitude of 7−8% of the total NADH. Abortive complex formation with dTDP-xylose either does not occur or happens so slowly that it is not observed over several hours.

The most interesting difference between these two compounds is the amount of NADH formed in the first phase of their reactions (7−8% for dTDP-6-deoxyglucose/galactose vs 73% for dTDP-xylose). While it is true that the dTDP-6-deoxyglucose/galactose is a mixture of two species that will have different reactivities, such a large variation in the amount of NADH indicates the importance of subtle differences in the hexose moiety to the position of this equilibrium. It is clear from this comparison that notable variances between dTDP-xylose and dTDP-6-deoxyglucose/galactose behavior make a direct comparison to the dTDP-glucose reaction untenable. An analysis of the first step in the reaction was performed using dTDP-xylose because abortive complex formation does not interfere, and because it appears to shift the equilibrium to favor formation of the observed NADH chromophore (increasing the sensitivity).

pH Profiles with dTDP-Xylose. The NADH levels for each variant with saturating dTDP-xylose were measured over a range of pH values. All of the 4,6-dehydratase variants fall into two groups with respect to the overall shape of their pH profiles. The first group consists of $D135A^{DEH}$, $E136Q^{DEH}$, $E136A^{DEH}$, and the double variant $D135N/E136Q^{DEH}$, in panel A; $Y301F^{DEH}$ in panel B; and $C187A^{DEH}$, $C187S^{DEH}$, and $H232N^{DEH}$ in panel C. It is similar to wt in that each member has a 60−80% NADH plateau at high pH, and that value drops off below pH 7. $Y301F^{DEH}$ is exceptional as it shows a decrease in the fraction of NADH from 80% to 50% above pH 9.5. Additionally, the fractions of NADH in $E136A^{DEH}$ and $C187A^{DEH}$ do not decrease dramatically at low pH but actually climb above the observed values for wt. The slight differences between the profiles for this group of variants may lead one to conclude that these residues do not have an important effect on the pH dependence of the equilibrium of the first step. The second group of variants includes $D135N^{DEH}$ from panel A; $K199R^{DEH}$, $K199M^{DEH}$, and $E198Q^{DEH}$ from panel B; and $H232Q^{DEH}$, $N190D^{DEH}$, and $N190A^{DEH}$ from panel C. These variants have a much lower fraction of NADH than wt over most of the pH range, but gradually merge with the first group at high pH. While all of these variants show a 5−10-fold drop in the fraction of NADH below wt values, they still show the same general pattern of pH dependence as wt. Presumably, some other ionizable residue(s) is (are) important for maintaining a high equilibrium fraction of NADH with dTDP-xylose.

Profiles indicate the importance of an unprotonated species with a pK_A between 6.0 and 7.0 in wt and in variants, which is not included among the residues tested in this study. Similarities between 4,6-dehydratase and 4-epimerase support the theory that this species is the $Tyr160^{DEH}$ anion. Like its homologous counterpart in 4-epimerase $Tyr149^{EPIM}$, $Tyr160^{DEH}$ is likely to have a pK_A between 6.0 and 7.0 (*21*). Given its close proximity to the NAD^+, it will certainly have a profound effect on the cofactor's reactivity.

Rate Constants for Dehydrogenation of dTDP-Xylose. The rates of NADH formation when variant 4,6-dehydratases were mixed with dTDP-xylose were measured at pH 7.5. Because these experiments were performed at saturating dTDP-xylose concentrations, this value represents the sum of k_3^{XYL} and k_4^{XYL} ($k_{obs} = k_3^{XYL} + k_4^{XYL}$). The NADH levels with dTDP-xylose represent the equilibrium of those same rate constants $\{E_{NADH}/E_{total} = k_3^{XYL}/(k_3^{XYL} + k_4^{XYL})\}$. These values were obtained and used to solve directly for k_3^{XYL} and k_4^{XYL} (Table 5). As was shown above, small variations in the substrate profoundly affect the equilibrium of the dehydrogenation step; thus, the values for k_3^{XYL} and k_4^{XYL} listed in Table 5 could not be used to draw conclusions about the analogous rate constants in the mechanism with the natural substrate. Comparisons *can* be made between wt and variant 4,6-dehydratase species *within this data set* to gain information about each active site variation on this first chemical step.

Three variants, $E198Q^{DEH}$, $K199R^{DEH}$, and $K199M^{DEH}$, stand out in Table 5 as displaying extensive, 3−4 orders of magnitude decrements in k_3^{XYL} and k_4^{XYL} from wt. All of the activity lost in k_{cat} (100−300-fold) can easily be accounted for by effects on the first step, even with considerable masking by contributions from other steps to the overall rate limitation. For $N190D^{DEH}$, one cannot account

for all of the decrease in k_{cat} (441-fold below wt) observed, though it displays the fourth largest drop in k_3^{XYL} (146-fold below wt). When one considers masking by slower steps, the discrepancy becomes even larger. For other variants, the effects are smaller; other decreases in k_3^{XYL} and k_4^{XYL} are around 10-fold (or less) below wt and are unlikely to contribute significantly to the observed drop in k_{cat} below that of wt for each variant.

Summary. We have developed a model of the active site of 4,6-dehydratase, and used it to rationalize mutagenesis of eight residues. From steady-state kinetic parameters, seven of those residues are clearly important for catalysis. While most of the variants show significant drops in k_{cat} and k_{cat}/K_M, it has proven difficult to assign the loss in activity to specific steps in catalysis. For the bulk of the residues investigated in this study, we have succeeded in narrowing the selection of steps which might be affected in each variant using a variety of steady-state techniques. Further characterization using the pre-steady-state rapid mix-quench MALDI technique (*7*) will be valuable for the analysis of two of the variants ($D135A^{DEH}$ and $Y301F^{DEH}$) as is apparent from NADH levels during steady-state turnover. We are currently pursuing the kinetics of isotopic exchange to try to determine the catalytic consequences of mutations at $Asp135^{DEH}$, $Glu136^{DEH}$, $Asn190^{DEH}$, $His232^{DEH}$, and $Tyr301^{DEH}$.

ACKNOWLEDGMENT

We thank Professor Brian Fox for use of the stopped-flow spectrophotometer. Circular dichroism spectra were obtained under the guidance of Dr. Darrell McCaslin at the University of Wisconsin−Madison Biophysics Instrumentation Facility, which is supported by the University of Wisconsin−Madison and by Grants BIR-9512577 (NSF) and S10 RR13790 (NIH). We also thank Dr. Martha M. Vestling for use of the University of Wisconsin−Madison Department of Chemistry's Bruker REFLEX II MALDI-TOF, which was purchased with the help of Award 9520868 (NSF).

NOTE ADDED IN PROOF

Following submission of this manuscript an article was published describing the crystal structure of 4,6-dehydratase from *Salmonella enterica* (*30*).

SUPPORTING INFORMATION AVAILABLE

Sequences of pairs of oligonucleotide primers for each 4,6-dehydratase variant (2 pages). This material is available free of charge via the Internet at http://pubs.acs.org.

REFERENCES

1. Glaser, L., and Kornfeld, S. (1961) *J. Biol. Chem. 236*, 1795−1799.
2. Liu, H.-W., and Thorson, J. S. (1994) *Annu. Rev. Microbiol. 48*, 223−256.
3. Giraud, M.-F., and Naismith, J. H. (2000) *Curr. Opin. Struct. Biol. 10*, 687−696.
4. Floss, H. G., Keller, P. J., and Beale, J. M. (1986) *J. Nat. Prod. 49*, 957−970.
5. Hutchinson, C. R. (1994) *Bio/Technology 12*, 375−380.
6. Glaser, L., and Zarkowsky, H. (1973) *The Enzymes* (Boyer, Ed.) Vol. 5, pp 465−480, Academic Press, New York.
7. Gross, J. W., Hegeman, A. D., Vestling, M. M., and Frey, P. A. (2000) *Biochemistry 39*, 13633−13640.
8. Wang, S. F., and Gabriel, O. (1970) *J. Biol. Chem. 245*, 8−14.
9. Zarkowski, H., Lipkin, E., and Glaser, L. (1970) *J. Biol. Chem. 245*, 6599−6606.
10. Jornvall, H., Persson, B., Krook, M., Atrian, S., Gonzalez-Duarte, R., Jeffery, J., and Ghosh, D. (1995) *Biochemistry 34*, 6003−6013.
11. Bauer, A. J., Rayment, I., Frey, P. A., and Holden, H. M. (1992) *Proteins: Struct., Funct., Genet. 12*, 372−381.
12. Liu, Y., Vanhooke, J. L., and Frey, P. A. (1996) *Biochemistry 35*, 7615−7620.
13. Moffatt, J. G. (1966) *Methods Enzymol. 8*, 136−142.
14. Okazaki, R., Okazaki, T., Strominger, J. L., and Michelson, A. M. (1962) *J. Biol. Chem. 237*, 3014−3026.
15. Harris, D. C. (1991) *Quantitative Chemical Analysis*, Third ed., p 102, W. H. Freeman and Co., New York.
16. Thompson, J. D., Higgins, D. G., and Gibson, T. J. (1994) *Nucleic Acids Res. 22*, 4673−4680.
17. Stein, A., Kula, M.-R., Elling, L., Verseck, S., and Klaffke, W. (1995) *Angew. Chem., Int. Ed. Engl. 34*, 1748−1749.
18. Thoden, J. B., Frey, P. A., and Holden, H. M. (1996) *Biochemistry 35*, 5137−5144.
19. Snipes, C. E., Brillinger, G. U., Sellers, L., Mascaro, L., and Floss, H. G. (1977) *J. Biol. Chem. 252*, 8113−8117.
20. Drenth, J., Jasonius, J. N., Koekoek, R., Swen, H. M., and Wolthers, B. G. (1968) *Nature 218*, 929−932.
21. Liu, Y., Thoden, J. B., Kim, J., Berger, E., Gulick, A. M., Ruzicka, F. J., Holden, H. M., and Frey, P. A. (1997) *Biochemistry 36*, 10675−10684.
22. Somoza, J. R., Menon, S., Schmidt, H., Joseph-McCarthy, D., Dessen, A., Stahl, M. L., Somers, W. S., and Sullivan, F. X. (2000) *Structure 8*, 123−135.
23. Davis, J. E., Nolan, L. D., and Frey, P. A. (1974) *Biochim. Biophys. Acta 334*, 442−447.
24. Swanson, B. A., and Frey, P. A. (1993) *Biochemistry 32*, 13231−13236.
25. Glaser, L. (1973) *The Enzymes* (Boyer, Ed.) Vol. 5, pp 355−380, Academic Press, New York.
26. Zarkowski, H., and Glaser, L. (1969) *J. Biol. Chem. 244*, 4750−4756.
27. Cleland, W. W. (1982) *CRC Crit. Rev. Biochem. 13*, 385.
28. Cleland, W. W. (1975) *Biochemistry 14*, 3220−3225.
29. Smith, T. J. (1995) *J. Mol. Graphics 13*, 122−125.
30. Allard, S. T. M., Girard, M.-F., Whitfield, C., Graninger, M., Messner, P., and Naismith, J. H. (2001) *J. Mol. Biol. 307*, 283−295.

BI010441A